AFS Proceedings 2011 © American Foundry Society, Schaumburg, IL USA

Mechanical Properties of Al-Si-Cu-Mg Cast Alloys: Effects of Tramp Elements

M.F. Ibrahim, E. Samuel, A.M. Samuel
Université du Québec à Chicoutimi, Chicoutimi, QC, Canada

A.M.A. Mohamed, F.H. Samuel
Université du Québec à Chicoutimi, Chicoutimi, QC, Canada
Suez Canal University, Suez, Egypt

A.M.A. Al-Ahmari
King Saud University, Riyadh, Saudi Arabia

ABSTRACT

Critical automotive applications using heat-treatable alloys are designed for high values of mechanical properties, which can be improved using a specified heat treatment. Castings were prepared from both experimental and industrial 319 alloy melts containing 0 to 0.6wt% Mg. Impact test bars were cast in two different cooling rate molds, namely a star-like permanent mold and an L-shaped permanent mold, with DASs of 24 μm and 50 μm, respectively. Tensile test bars were cast in an ASTM B108 permanent mold with a DAS of 25 μm. The bars were tempered at 180C (356F) and 220C (428F) for 2-48 hours. The results showed that Mg content, aging conditions, and cooling rate have a significant effect on the microstructure of both experimental and industrial alloys and, consequently, on the mechanical properties. The addition of Mg resulted in the precipitation of the β-Mg_2Si, Q-$Al_5Mg_8Cu_2Si_6$, π-$Al_8Mg_3FeSi_6$ and of the block-like θ-Al_2Cu phases. The presence of Mg and Cu, as well as the higher cooling rates improved the alloy strength, ductility, and hardness values, especially in the T6 heat-treated condition. As a result of this treatment, the alloys show hardening after up to 24 hours of aging time because of the influence of several hardening phases. The activity of Cu significantly lowers the impact properties, which are determined mainly by the Al_2Cu phase and not by the eutectic Si particles. The addition of Mg was also seen to diminish the effects of impact toughness. The crack initiation energy in these alloys is greater than the crack propagation energy, reflecting the high ductility of Al-Si-Cu-Mg base alloys. Applying aging at 220C, (428F) causes overaging and alloy softening after 2 hours of aging time. The experimental alloys demonstrate higher values of mechanical properties than the industrial alloys.

Key Words: Al-Si-Cu-Mg Alloys, Cooling rate, Alloying elements, Heat treatment, Microstructure, Mechanical properties.

INTRODUCTION

Aluminum alloys are widely used nowadays in the automotive industry, since recent trends incline toward achieving higher performance without increasing weight. Automotive components are thus increasingly being made of aluminum alloys in order to reduce overall weight, while at the same time maintaining or improving mechanical properties. Apart from their excellent casting characteristics, with their wear and corrosion resistance, aluminum-silicon (Al-Si) casting alloys are used extensively because they also impart a wide range of mechanical properties and high strength-to-weight ratio.[1]

Alloy 319 is one of the main alloys of the hypoeutectic Al-Si group. The as-cast microstructure of 319 alloys consists of the Al matrix (α-Al dendrites, silicon particles, intermetallic phases, nonmetallic inclusions, and porosity); it is controlled by chemical composition, melt treatment conditions, solidification rate, and the heat treatment applied.

Copper results in the precipitation of Al_2Cu particles; depending on cooling rate and modifier level, this phase could appear as blocklike and/or fine eutectic Al-Al_2Cu colonies in the microstructure.[2] It should be noted that the block-like Al_2Cu does not dissolve during heat treatment.[3] When the brittle Al_2Cu phase is present, fracture is no longer controlled by the Si particles. Although the eutectic Si has been Sr-modified, the impact strength does not improve. Moreover, there is a tendency to form more block-like Al_2Cu, in the presence of Sr, which contributes to the noticeably low impact strengths in 319 alloys.[3,4]

The addition of Mg will increase the strength values during aging due to the precipitation of submicroscopic and metastable phases containing Mg and Si, which provide excellent obstacles for dislocation movement. The addition of up to 0.5 wt% Mg to molten 319-type alloys leads to the precipitation of Mg_2Si, a Mg-rich phase, in the form of rounded black particles dotted along the sides of the eutectic Si particles.

The hardness of the 319 alloys increases with the addition of Mg and the α-Fe intermetallics volume fraction, although it decreases with Sr modification and aging parameters. The contribution of Mg to increasing the hardness of heat-treated 319 alloys containing β-Fe intermetallics is more noticeable than it is for the 319 alloys containing α-Fe intermetallics.[5] The addition of Mg and Cu improves the hardness and strength of the 319 alloys; the Cu-containing alloys, however, are less sensitive to the presence of Sr.[6] The 319 alloy hardness first increases with an increase in aging temperature of up to 180C (356F), and thereafter decreases as the aging temperature is increased.[7]

The Mg content also affects the type and total volume fraction of Fe-bearing phases, especially in Be-free alloys. The iron-rich intermetallic phases in the low-Mg alloy are almost exclusively small β-phase (Al_5FeSi) plates. Large π-phase ($Al_8Mg_3FeSi_6$) particles, however, are dominant in the high-Mg alloy, together with a small proportion of the β-phase.[8-10]

Iron is always present in commercial Al-Si alloys and has consistently emerged as the main impurity element which is perhaps the most detrimental to the mechanical properties of these alloys. Iron forms different types of intermetallic compounds during solidification, *e.g.* the platelet-like β-Al_5FeSi and the script-like α-$Al_{15}(Mn,Fe)_3Si_2$ phases. In the solidification process, β-Al_5FeSi platelets are active sites for the nucleation of the Al_2Cu phase. The addition of Mg leads to the formation of the π-$Al_8Mg_3FeSi_6$ phase. Under cooling rates close to equilibrium conditions for multi-component 3xx alloys and at ~540C (1004F), the Mg_2Si and π-$Al_8Mg_3FeSi_6$ phases begin to precipitate. When the temperature is lowered to 490-530C (914-986F), precipitation of the Al_2Cu and Q-$Al_5Mg_8Cu_2Si_6$ phases occurs.[11] A complete dissolution of the iron intermetallics seems to be less likely since the solubility of iron in the aluminum matrix is negligible, thus, the iron intermetallics only transform from one phase to another, though a certain amount of fragmentation and spheroidization may occur.[12-14]

Cooling rate has a direct effect on the shape, size, and distribution of the microstructural phases, as well as on the aluminum dendrites, eutectic Si, and pore size. Iron intermetallics also vary greatly in size and composition as a function of the cooling rate and magnesium content.[4] The cooling rate is thus the most critical variable in controlling the size and distribution of the intermetallic phases and porosity.[15]

Most of the heat treatments recommended for 319 alloys restrict the solution temperature to below the final solidification point in order to avoid the melting of copper-containing phases. Solution heat treatment of Al-Si-Cu-Mg alloys is used to homogenize the alloy, to change the morphology of the interdendritic phases, and to dissolve precipitation-hardening constituents, such as Al_2Cu, Al_2MgCu, and Mg_2Si.[16] Yang[17] recommended a solution heat treatment temperature guideline for experimental and industrial 319 alloys to minimize the occurrence of incipient melting. The best combination of strength and ductility is obtained when the as-cast material is solution heat-treated at 515C (959F) for 8-16 hours, followed by a 60C (140F) warm water quench. A higher solution temperature results in the partial melting of the copper phase at the grain boundaries.[18,19] Aging is the final stage in the heat treatment of cast aluminum alloys. The effect of precipitation heat treatment on mechanical properties is greatly accelerated by heating the quenched Al-Si-Cu alloys in the range of 95-205C (203-401F).[20] The incipient melting of the $Al_5Mg_8Cu_2Si_6$ and Al_2Cu phases of the 319 alloys took place when the high-Mg version of 319 was solution heat-treated at temperatures above 505C (941F) for sufficiently long periods.[21]

The current work was undertaken to investigate the effects of Mg content, tramp elements, aging conditions, and cooling rate on the microstructure and mechanical properties of Al-Si-Cu-Mg base alloys. The characteristics of eutectic Si particles are herein examined and explained for both of the cooling rates.

EXPERIMENTAL PROCEDURES

Both industrial-commercial and experimental 319 alloys were used as a basis for the current study. The industrial B319 alloy was received in the form of 12.5 kg ingots. Samplings for chemical analysis were taken from each alloy melt which had previously been prepared. Table 1 lists the chemical analyses of the various experimental and industrial alloys studied and their respective codes, as obtained from samplings for the chemical analysis taken from the corresponding melts. With respect to the alloy codes, the prefix D represents the non-modified alloys using star-like mold, LD the non-modified alloys using L-shaped mold, and E and I the non-modified experimental and industrial alloys, respectively, using ASTM B108 mold. The numbers 1, 2, 3, 4, 5, and 6 correspond to the Mg levels of 0.0, 0.1, 0.2, 0.3, 0.4 and 0.6% for experimental alloys, respectively, while numbers 7 and 8 correspond to 0.3 and 0.6% Mg for industrial alloys, respectively. Finally, the suffix S in any code implies that alloy has been Sr-modified.

Table 1. Average Chemical Composition (wt %) of the Experimental and Industrial Alloys Studied

Alloy code	Element Concentration (wt %)							
	Si	**Fe**	**Cu**	**Mn**	**Mg**	**Zn**	**Ni**	**Al**
D1/E1 (or LD1)	6.76	0.201	3.812	0.0059	0.0081	0.0042	0.0114	Bal.
D2/E2 (or LD2)	6.59	0.1899	3.569	0.0065	0.1067	0.0044	0.0098	Bal.
D3/E3 (or LD3)	6.39	0.1815	3.465	0.0069	0.2384	0.0050	0.0096	Bal.
D4/E4 (or LD4)	6.62	0.1822	3.562	0.0023	0.3219	< 0.0017	0.0100	Bal.
D5/E5 (or LD5)	6.64	0.1847	3.606	0.0030	0.4256	< 0.0017	0.0099	Bal.
D6/E6 (or LD6)	6.66	0.1890	3.564	0.0034	0.636	< 0.0017	0.0092	Bal.
D7/I7 (or LD7)	7.43	0.3197	3.314	0.2874	0.3376	0.1255	0.0452	Bal.
D8/I8 (or LD8)	7.47	0.3138	3.375	0.2847	0.643	0.1260	0.0449	Bal.

Measured additions of Mg and Sr were made to the melt. Strontium was added in the form of the Al-10%Sr master alloy to obtain 200 ppm Sr levels, whereas Mg was added in the form of the pure metal. Prior to casting, the molten metal was degassed for 15 minutes using pure, dry argon to remove the hydrogen and inclusions. Various 319 alloys were used to prepare castings from which test bars were obtained for mechanical testing. With this aim in mind, the molten metal was poured into a permanent mold, which had been preheated to 450C (842F).

Each mold-type was selected for a particular intrinsic quality to prepare hardness test samples and to take metallographic measurements. Figures 1(a) and (b) show the L-shaped and star-like molds were used for low and high cooling rate, respectively. After the test bars were cut from the casting, they were machined to the required specifications.

The test bars were prepared for each alloy composition and divided into sixteen sets, with one set kept in the as-cast condition and one set solution heat-treated at 495C (923F) for 8 hours, then quenched in warm water at 65C (149F). Seven sets of bars were solution heat-treated at 495C (923F) for 8 hours, then also quenched in warm water at 65C (203F) and artificially aged at 180C (356F) for 2, 4, 6, 8, 12, 24, and 48 hours, respectively; the remaining seven sets were solution heat-treated at 495C (923F) for 8 hours, quenched in 65C (149F) water and artificially aged at 220C (428F) for 2, 4, 6, 8, 12, 24, and 48 hours, respectively. For each heat treatment, five test bars were used.

Hardness test bars measuring 10 mm x 10 mm x 55mm were cut from the casting. The specimen surfaces were polished with fine sandpaper to remove any machining marks. The hardness measurements were carried out on the as-cast and heat-treated samples using a Brinell hardness tester, applying a steel ball of 10 mm diameter and a load of 500 kgf for 30 seconds. An average of four readings obtained from two perpendicular surfaces was taken to represent the hardness value in each case.

From each of these samples prepared for metallographic characterization, two samples measuring 10 x 10 mm, one as-cast and one solution heat-treated, were sectioned off to study each alloy condition. The microstructures of the polished sample surfaces were examined using an optical microscope linked to a Clemex image analysis system. The dendrite arm spacing (DAS) of both mold samples was measured applying the line intercept method. The eutectic Si particle characteristics, including area, length, aspect ratio, roundness, and density, were measured and quantified.

Impact test bars measuring 10 mm x 10 mm x 55 mm were prepared from the casting obtained from both the star-like mold and L-shaped mold. The surfaces of these samples were polished to remove any machining marks; it should be noted that the samples were used in the unnotched condition. All the samples were heat-treated using the same conditions as those applied to the samples used for hardness measurements. A computer-aided instrumented SATEC SI-1 Universal Impact Testing Machine (SATEC Systems Inc., Model SI-1D3) was used to carry out the impact testing. The total absorbed energy was determined, for which the average values of the energies obtained from the five samples tested for each alloy condition were taken to represent the impact energy value for that particular condition.

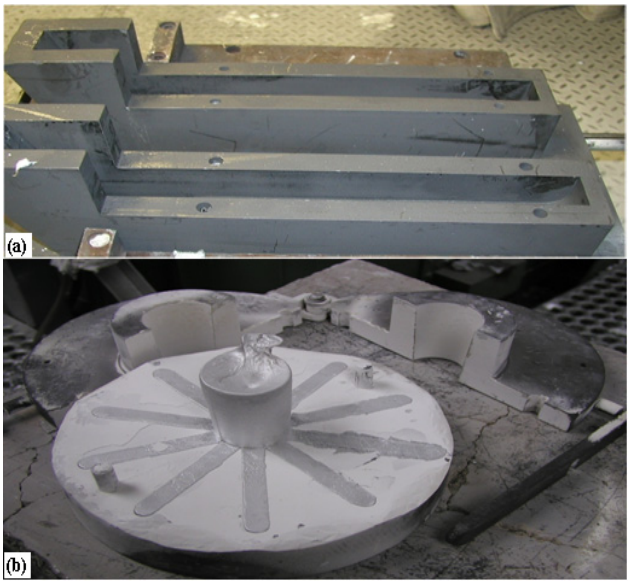

Fig. 1. Shows (a) L-shaped and (b) star-like molds used in this study.

Tensile test bars were prepared from the casting obtained from the ASTM B108 mold. All the samples were heat-treated using the same conditions as those applied to the samples used for hardness measurements and impact testing. Tensile testing was carried out for the as-cast and the heat-treated test bars at room temperature using an MTS Servohydraulic mechanical testing machine working at a strain rate of 1.0×10^{-4}/s. The elongation of the test specimens was measured using a strain gauge extensometer attached to the specimen during the tension test. A data acquisition system was attached to the MTS machine to provide the results of the tensile test. For each sample tested, a stress-strain curve was obtained to illustrate the mechanical behavior of each specimen under the loads applied. The tensile test results obtained from testing a specific specimen represent the data pertaining to elongation to fracture, yield strength at 0.2% offset strain, and ultimate tensile strength. Ten tensile test bars for each composition were tested in the as-cast and the heat-treated conditions.

RESULTS AND DISCUSSION

MICROSTRUCTURAL ANALYSIS

Tables 2-5 summarize silicon particle characteristics for both the experimental and industrial base alloys investigated in the as-cast and solution heat-treated conditions. Table 2 lists Si particle measurements for the D1 experimental Mg-free base alloy using the star-like mold with the higher cooling rate and a DAS of 24 µm. It will be observed that the Si particle area decreases from 29.60 to 5.22 µm^2, while its length decreases from 17 to 5.16 µm, and its aspect ratio decreases from 4.31 to 2.96, whereas its roundness ratio is observed to increase from 16.5 to 27% after Sr-modification. After solution heat treatment, the particle area decreases to 27.1 µm^2, the particle length, and aspect ratio both decrease to 12.5 and 3.92 µm, respectively, although the roundness ratio increases to 26.4% for the non-modified experimental base alloy D1. Also, with respect to the solution heat-treated and Sr-modified base alloy DS1, the particle area and length increase from 5.22 to 9.4 µm^2 and 5.16 to 5.64 µm, respectively, while the aspect ratio decreases from 2.96 to 2.54, as a result of Si particle coarsening. These results are in satisfactory agreement with those of Gruzleski and Closset,[4,22] Hatch,[23] Apelian,[24] and Moustafa *et al.*[6,25]

Table 2. Silicon Particle Measurements for the D1 Experimental Alloy using a Star-like Mold with a DAS of 24 µm

Alloy (Condition)	Area (µm^2)		Length (µm)		Roundness Ratio (%)		Aspect Ratio	
	Av.	SD	Av.	SD	Av.	SD	Av.	SD
D1 (non-modified)	29.60	23.80	17.00	10.90	16.5	8.6	4.31	2.21
DS1 (Sr-modified)	5.22	4.78	5.16	3.09	27.0	9.6	2.96	0.99
D1 (non-mod. + SHT)	27.10	20.80	12.50	7.50	26.4	11.3	3.92	1.96
DS1 (Sr-mod. + SHT)	9.40	6.06	5.64	2.33	36.7	8.0	2.54	0.59

Av: Average, SD: Standard Deviation

Table 3 summarizes the silicon particle characteristics of the same experimental base alloy, namely alloy LD1, using an L-shaped mold with the lower cooling rate and a DAS of 50 µm. The silicon particle size in this case was observed to increase as a direct effect of the slow solidification rate.

Table 3. Silicon Particle Measurements for the LD1 Experimental Alloy using an L-Shaped Mold with a DAS of 50 µm

Alloy (Condition)	Area (µm^2)		Length (µm)		Roundness Ratio (%)		Aspect Ratio	
	Av.	SD	Av.	SD	Av.	SD	Av.	SD
LD1 (non-modified)	72.00	68.70	25.00	16.00	17.2	8.8	4.14	2.12
LDS1 (Sr-modified)	4.51	3.60	4.58	2.45	29.5	9.6	2.89	0.93
LD1 (non-mod. + SHT)	61.50	49.60	19.70	12.50	23.6	10.5	3.85	1.78
LDS1 (Sr-mod. + SHT)	10.80	7.29	6.22	2.71	35.1	8.4	2.65	0.66

Table 4 summarizes the Si particle characteristics of the D7 industrial base alloy containing 0.3wt% Mg when using the higher cooling rate star-like mold. Compared to the Si particle characteristics observed for the D1 experimental base alloy, the Si particle characteristics in the D7 alloy increase as a direct effect of chemical composition, specifically the increased Mg content and the impurities present in the industrial alloy.

Table 4. Silicon Particle Measurements for the D7 Industrial Alloy using a Star-like Mold

Alloy (Condition)	Area (μm²)		Length (μm)		Roundness Ratio (%)		Aspect Ratio	
	Av.	SD	Av.	SD	Av.	SD	Av.	SD
D7 (non-modified)	34.85	40.75	14.46	11.80	26.5	15.7	3.96	1.94
DS7 (Sr-modified)	4.87	4.19	4.84	2.48	27.2	8.5	2.65	0.64
D7 (non-mod. + SHT)	33.55	35.15	12.85	8.78	33.5	15.6	3.55	1.68
DS7 (Sr-mod. + SHT)	10.10	6.49	5.80	2.33	36.4	7.3	2.47	0.50

Table 5 summarizes the Si particle characteristics of the LD7 industrial base alloy containing 0.3wt% Mg when using the lower cooling rate L-shaped mold. As a result of using this mold, the silicon particle size and characteristics increase as a direct effect of the slow cooling rate.

Table 5. Silicon Particle Measurements for the LD7 Industrial Alloy using the L-shaped Mold

Alloy (Condition)	Area (μm²)		Length (μm)		Roundness Ratio (%)		Aspect Ratio	
	Av.	SD	Av.	SD	Av.	SD	Av.	SD
LD7 (non-modified)	73.00	73.70	24.40	16.30	17.7	8.8	3.91	1.93
LDS7 (Sr-modified)	6.21	5.01	5.74	3.40	26.9	10.2	3.10	1.17
LD7 (non-mod. + SHT)	64.50	83.80	20.55	16.90	27.7	10.4	3.83	1.87
LDS7 (Sr-mod. + SHT)	11.60	8.13	6.31	2.77	35.5	8.3	2.61	0.68

The Si particle characteristics of the E1 experimental Mg-free base alloy using the ASTM B108 mold with a DAS of 25 μm closely approach those of the D1 experimental Mg-free base alloy using the star-like mold with the higher cooling rate and a DAS of 24 μm, as summarized in Table 2. The Si particle characteristics of the I7 industrial base alloy containing 0.3wt% Mg when using the ASTM B108 mold closely approach those of the D7 industrial base alloy containing 0.3wt% Mg when using the higher cooling rate star-like mold, as summarized in Table 4.

The cooling rate is one of the most significant variables in controlling the size and distribution of the intermetallic phases. When comparing the microstructures in Figures 2(a) and (b), the size of these intermetallics increases with a decrease in the cooling rate. These observations are in satisfactory agreement with the ones reported by Samuel *et al.*[15]

The effects of modification, solution heat treatment, and Mg content with regard to Si particles and intermetallic compounds in the microstructures of the D7 industrial alloys containing 0.3wt% Mg;the D8 industrial alloy containing 0.6wt% Mg, (iii) the LD6 experimental alloy containing 0.6wt% Mg, (iv) the LD7 industrial alloys containing 0.3wt% Mg, and (v) the LD8 industrial alloy containing 0.6wt% Mg are all similar to those observed for the D1 and D6 experimental alloys. In addition to the copper and iron intermetallic compounds, the Mg_2Si phase may be observed in the as-cast microstructures of both the experimental and industrial alloys containing up to 0.6wt% Mg. In Figure 3, the presence of ultrafine Si particles within the Al-Al_2Cu eutectic structure may also be observed, tending to precipitate at the end of the solidification process; the encircled area 2 in Figure 3(b) shows these ultrafine Si particles. Remnants of undissolved Al_2Cu after solution heat treatment may also be noted in Figure 3(a). In addition, examples of the ultrafine β-phase platelets observed in the microstructure of the solution heat-treated sample of the LD7 alloys are shown in the encircled areas numbered 1 and 2 in Figure 3(b). Fine remnants of the mostly dissolved π-$Al_8Mg_3FeSi_6$ phase are shown in the encircled area 3 of this figure also. The large standard deviation observed is due the presence of extremely large Si particles indicated by the thick solid arrow shown in Figure 3(b) adjacent to relatively fine ones indicated by the broken arrow.

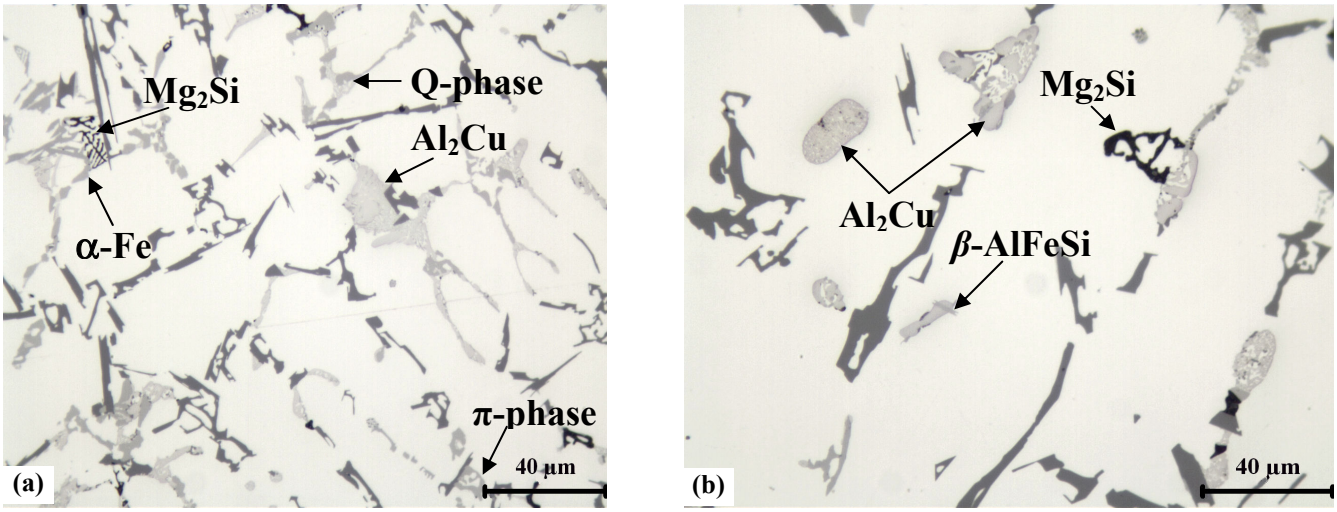

Fig. 2. Optical microstructures observed in the D8 industrial alloy samples containing 0.6wt%Mg obtained from: (a) a star-like mold casting (D8 alloy), and (b) an L-shaped mold casting (LD8 alloy).

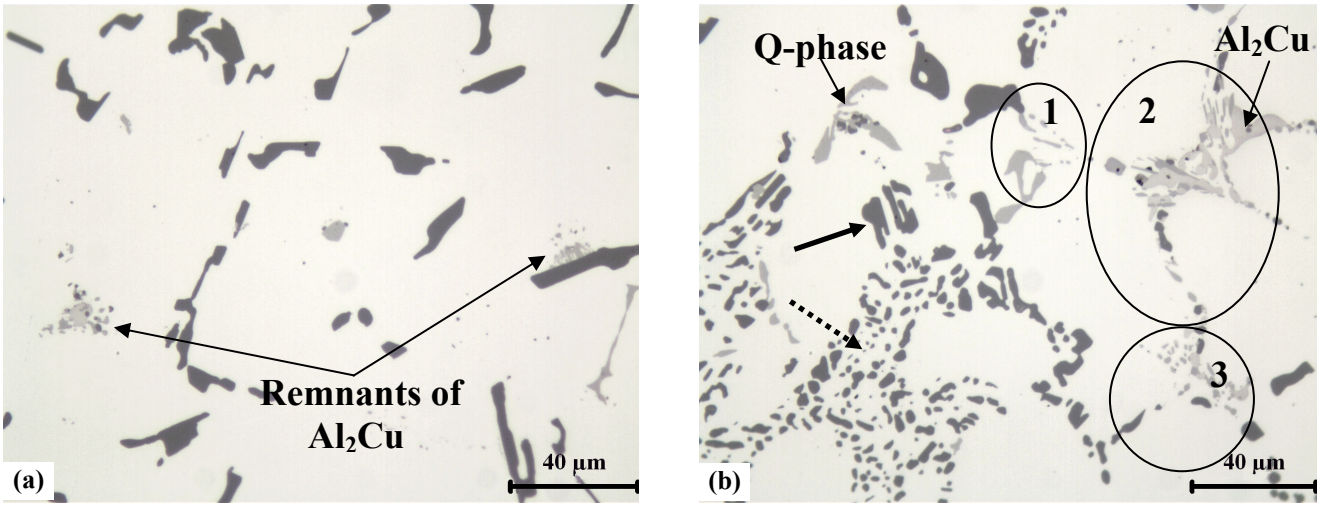

Fig. 3. Optical microstructures observed in solution heat-treated LD7 industrial alloy samples obtained from L-shaped mold castings: (a) non-modified alloy LD7, and (b) Sr-modified alloy LDS7.

HARDNESS

Table 6 summarizes the hardness values of the experimental and industrial as-cast 319 alloys for non-modified samples obtained out of the star-like, ASTM B108, and L-shaped molds, coded D, E/I, and LD, respectively. It was found that the hardness increases with an increase in both the Mg content and the cooling rate for both the experimental and industrial alloys.

Table 6. Hardness Values of the Experimental and Industrial As-cast 319 Alloys

Alloy	Hardness (BHN)		Alloy	Hardness (BHN)	
	Av.	SD		Av.	SD
D1/E1	71.4	2.1	LD1	73.8	0.7
D2/E2	83.8	4.2	LD2	81.4	2.3
D3/E3	88.8	2.0	LD3	88.1	1.6
D4/E4	90.9	3.8	LD4	89.8	1.4
D5/E5	92.8	1.9	LD5	94.4	1.9
D6/E6	94.5	2.9	LD6	97.3	2.7
D7/I7	94.4	2.8	LD7	95.0	0.4
D8/I8	98.9	2.8	LD8	95.9	5.1

The effects of Mg addition on the hardness of T6 heat-treated non-modified experimental 319 alloys were investigated as a function of aging time, and shown in Figures 4 and 5 for samples obtained from the star-like and L-shaped molds, respectively. Figure 4 shows the Brinell hardness values for non-modified experimental alloys, including the highest recorded Brinell hardness value of all the alloys tested here, namely, 143.52 BHN for the non-modified experimental alloy D4 containing 0.3wt% Mg. This group of curves was obtained using the higher cooling rate starlike mold samples. It was found that alloy hardness values could be increased by increasing the Mg content. Thus, regular and successive increases of the Mg content in the D1 Mg-free base alloy, for example, by 0.1wt% created the D2 alloy; by 0.2wt% created the D3 alloy; by 0.3wt% created the D4 alloy; by 0.4wt% created the D5 alloy; and by 0.6wt% created the D6 alloy, thereby increasing the alloy hardness values by ~32%, ~43%, ~46%, ~42% and ~42%, respectively.

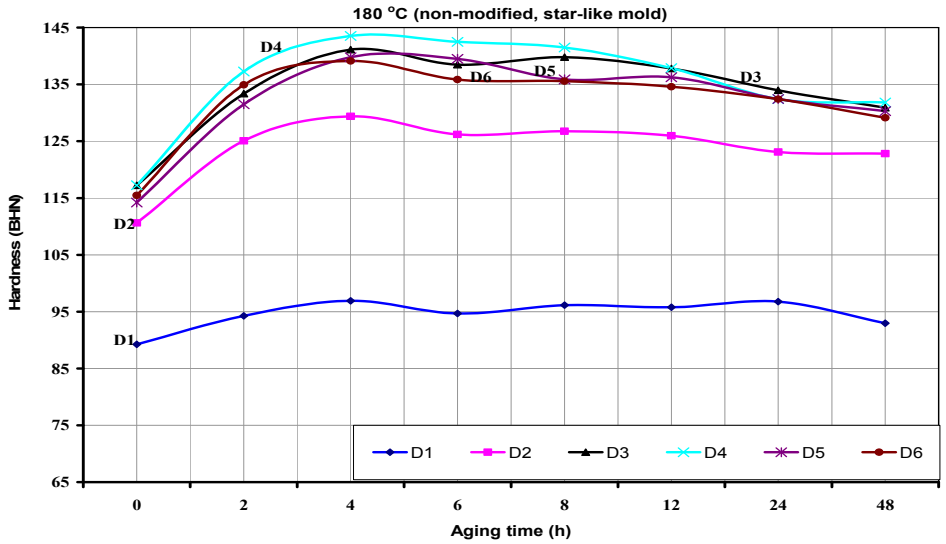

Fig. 4. Hardness of T6-tempered experimental 319 alloys at an aging temperature of 180C (356F) as a function of aging time, using the star-like mold samples of non-modified alloys.

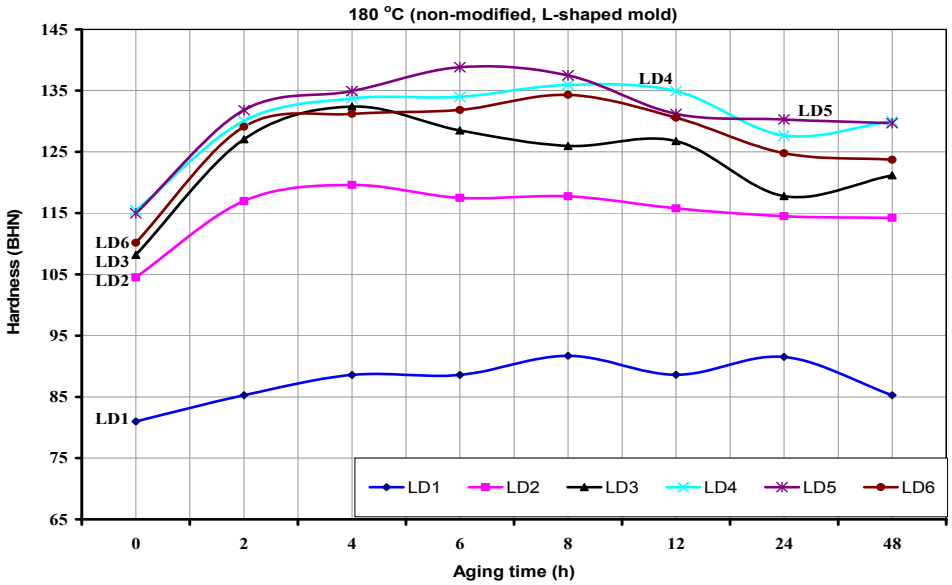

Fig. 5. Hardness of T6-tempered experimental 319 alloys at an aging temperature of 180C (356F) as a function of aging time, using the L-shaped mold samples of non-modified alloys.

It was also observed that an increase in the Mg content, of up to 0.4wt%, at different aging times produces a positive effect on hardness, indicating that hardening is due to Mg_2Si precipitation, in addition to the precipitation of Al_2Cu. The effects of Mg in aged alloys are similar to those observed in the as-cast alloys. Aging of these Mg-

containing 319 alloys at 180C (356F) in T6 heat treatment conditions for up to 48 hours produces a sharp rise in hardness values during the first two hours of aging, followed by a broad peak or plateau spread between 2 and 12 hours, as well as a noticeable period of over-aging beyond 12 hours. The lower cooling rate L-shaped mold was used to investigate the effects of cooling rate on the hardness of the experimental 319 alloys, as shown in Figure 5. When compared to Figure 4, it will be seen that the slow cooling rate diminishes the hardness values in both the non-modified and Sr-modified T6 heat-treated alloys. The effects of Mg addition on the hardness of the non-modified experimental 319 alloys as a function of aging time were also investigated under T7 heat treatment conditions, and are shown in Figures 6 and 7 for samples obtained from the star-like and L-shaped molds, respectively. Similar observations were noted in the case of the T6 heat-treated alloys, as shown in Figures 4 and 5. Aging of these Mg-containing experimental 319 alloys at 220C (428F) in T7 heat treatment conditions for up to 48 hours produces a sharp rise in hardness during the first two hours of aging, followed by an aging peak and a noticeable period of over-aging, beyond 2 hours of aging.

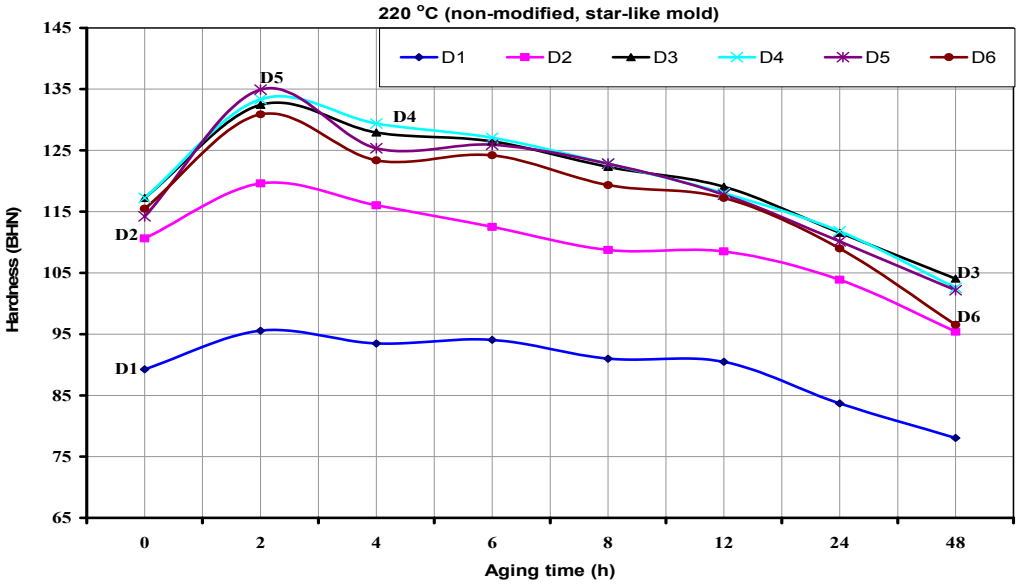

Fig. 6. Hardness of T7-tempered experimental 319 alloys at an aging temperature of 220C (428F) as a function of aging time, using the star-like mold sample of non-modified alloys.

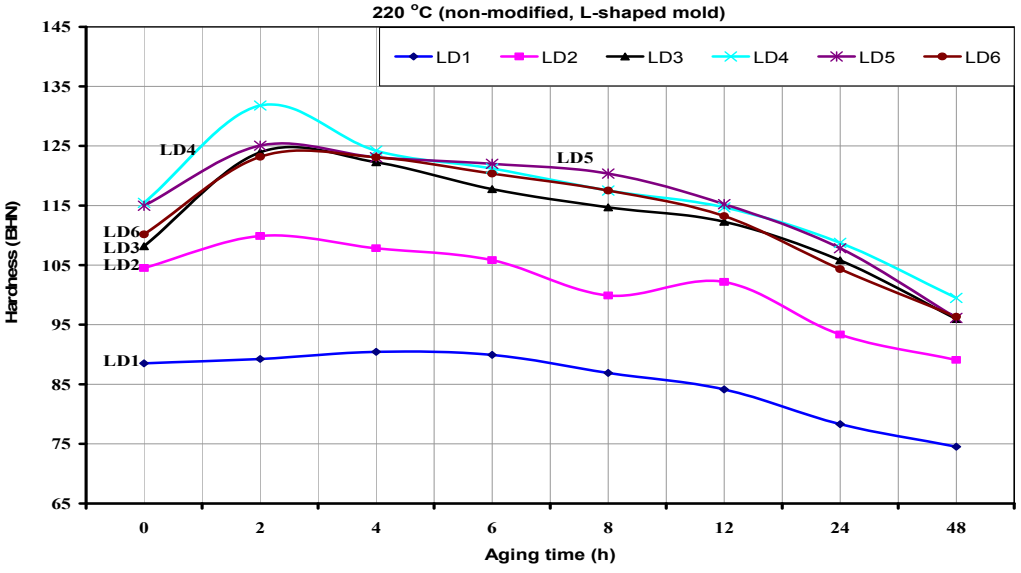

Fig. 7. Hardness of T7-tempered experimental 319 alloys at an aging temperature of 220C (428F) as a function of aging time, using the L-shaped mold samples of non-modified alloys.

The effects of the addition of Mg on the hardness of the non-modified industrial 319 alloys as a function of aging time were investigated under both T6 and T7 heat treatment conditions for samples obtained from the star-like and L-shaped molds, respectively. The results are provided in Figures 8 and 9. It was observed that both the Mg-containing industrial and experimental 319 alloys displayed similar behavior with respect to the influence of Mg-content, aging temperature (180C *vs* 220C) (356F *vs* 428F), and cooling rate (star-like mold *vs* L-shaped mold), as shown in Figures 4 through 9.

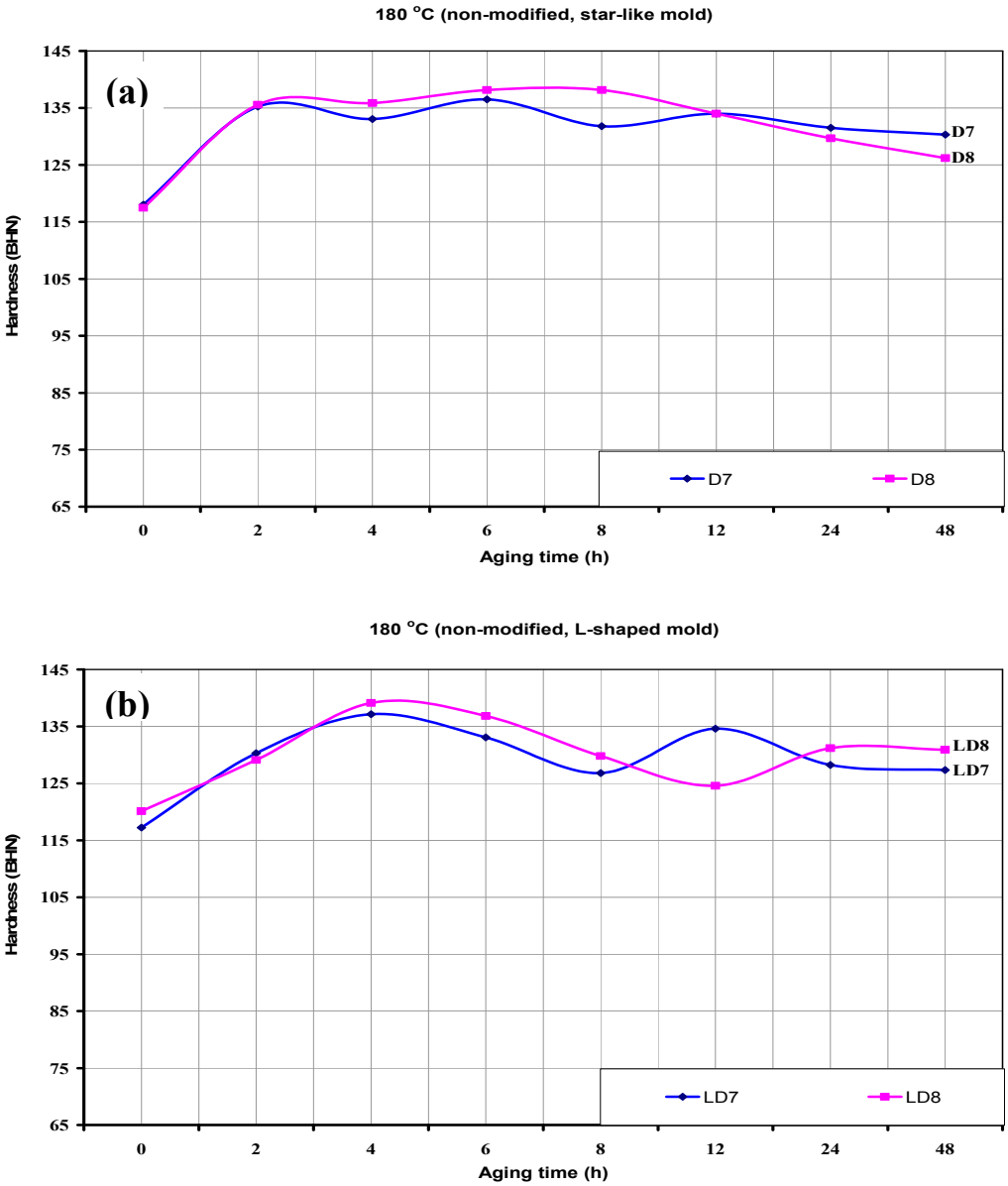

Fig. 8. Hardness of T6-tempered industrial non-modified 319 alloys at an aging temperature of 180C (356F) as a function of aging time for: (a) star-like mold samples and (b) L-shaped mold samples.

The hardness curves shown in Figures 4 to 9 display more than one peak or a wavy form with aging time; these results from the presence of several hardening phases, including θ-Al_2Cu, β-Mg_2Si, and Q-$Al_5Mg_8Si_6Cu_2$, and they contribute to the precipitation hardening of the alloys. Similar observations for this wavy form were recorded and explained for Al-Si-Cu-Mg 380 alloys by Morin,[26] based on two different types of structures that are likely be obtained during the aging treatment of 319 alloys.

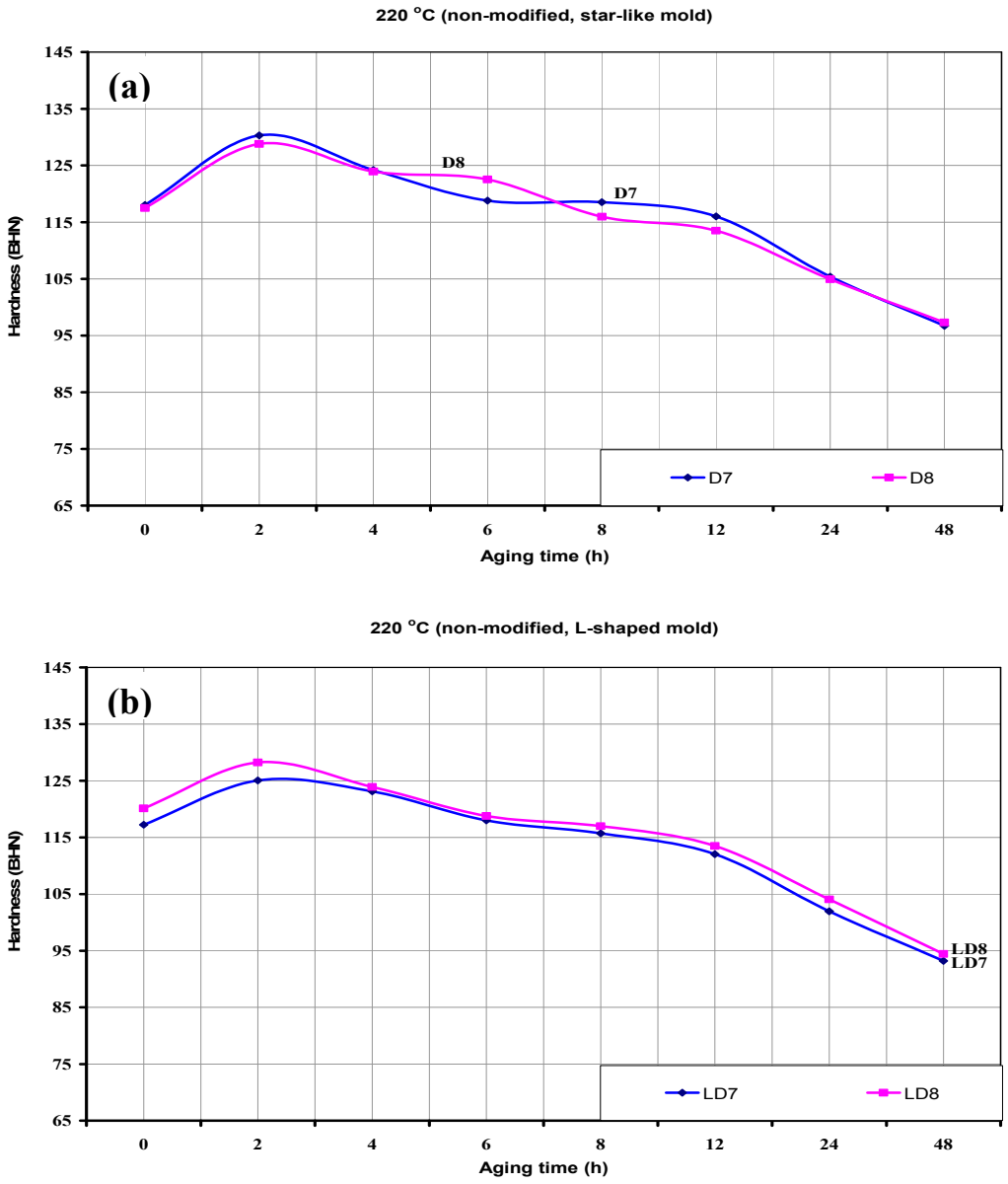

Fig. 9. Hardness of T7-tempered industrial non-modified 319 alloys at an aging temperature of 220C (428F) as a function of aging time for: (a) star-like mold samples and (b) L-shaped mold samples.

The negative effects of Sr-modification on the properties of 319 alloys involve the segregation of the brittle, block-like Al_2Cu in areas away from the modified Si particles. In addition to the *Q*-$Al_5Mg_8Cu_2Si_6$ phase, this blocklike Al_2Cu is known to be insoluble. Table 7 illustrates these undissolved Cu-rich phases, which control the properties, and the fracture behavior of the alloys investigated. Such an observation is in satisfactory agreement with data reported by Paray *et al.*[3,27]

Table 7 summarizes the volume fraction of Al_2Cu (%) for both the as-cast and solution heat-treated experimental 319 alloy in non-modified and Sr-modified conditions, as observed in the star-like and L-shaped mold samples. The volume fraction of Al_2Cu (%) for the Sr-modified alloy is higher than it is for the non-modified alloy in both the as-cast and solution heat-treated conditions. These volume fraction values confirm: (i) the negative effects of Sr modification on 319 alloys containing ~3.5% Cu, (ii) the decrease in hardness values of Sr-modified 319 alloys in both the as-cast and solution heat-treated conditions, and (iii) the hardness data summarized in Table 6 and those plotted in Figures 4 to 9. These observations are all in satisfactory agreement with those reported by Tash *et al.*[5,28], Moustafa *et al.*[6], and Paray *et al.*[3,27]

Table 7. Volume Fraction of Al2Cu (%) for the Base Alloy

Alloy	Volume Fraction of Al_2Cu (%)			
	As-Cast		SHT	
	Av.	SD	Av.	SD
D1	5.74	0.69	0.49	0.09
DS1	4.87	0.95	1.82	0.58
LD1	4.19	0.38	0.93	0.18
LDS1	4.27	0.45	2.15	0.63

The effects of aging temperature on the hardness of the non-modified experimental 319 alloys as a function of Mg content were also investigated for both molds, with the results provided in Figure 10. It was found that alloy hardness values could be increased by increasing the Mg content. Thus, increasing the Mg content by up to 0.3wt% increased hardness values noticeably. Increasing Mg content beyond 0.3 wt%, *i.e* up to 0.6 wt%, did not lead to any noticeable increase in the alloy hardness. The decline observed in the hardness values beyond 0.3wt% Mg may be attributed to the increase in the volume fraction of both π-$Al_8Mg_3FeSi_6$ and Q-$Al_5Mg_8Cu_2Si_6$ phases. Increasing the aging temperature up to 180C (356F) increased hardness values which thereafter decreased for both mold samples as the aging temperature was increased to 220C (428F). Similar observations were recorded for increasing Mg content and aging temperature in industrial 319 alloys. These observations are all in satisfactory agreement with those reported by Tash *et al.*[5,28], Moustafa *et al.*[6], and Mohamed.[7]

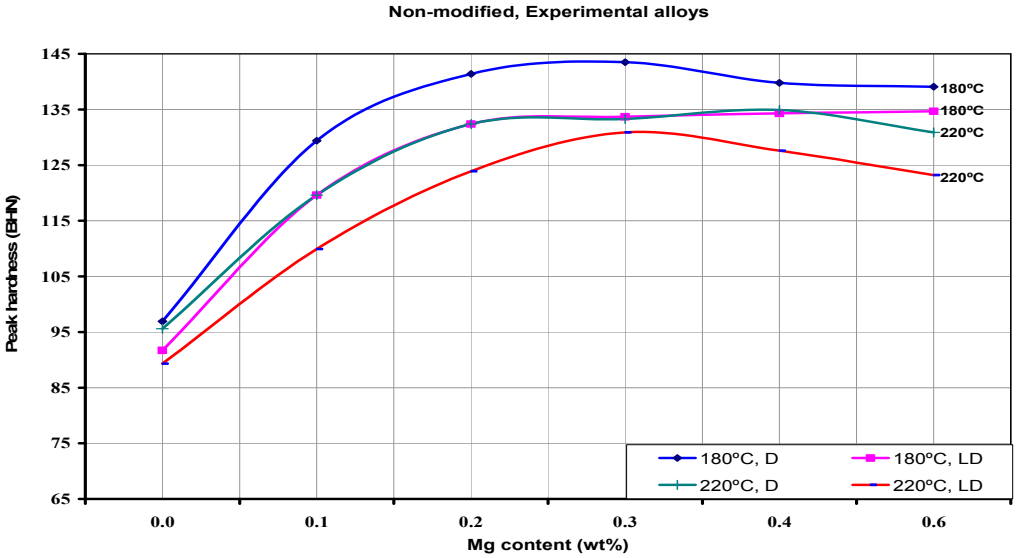

Fig. 10. Hardness of experimental non-modified 319 alloys for two aging temperatures and two molds as a function of Mg content (wt %).

TENSILE TESTING

Table 8 summarizes the tensile properties, namely, ultimate tensile strength (UTS), yield strength (YS), and elongation to fracture (EF), of the experimental and industrial as-cast 319 alloys for non-modified samples.

Table 8. Tensile Testing Values of the Experimental and Industrial As-cast 319 Alloys

Alloy	UTS (MPa)		Alloy	YS (MPa)		Alloy	EF (%)	
	Av.	SD		Av.	SD		Av.	SD
E1	244.04	12.16	E1	128.80	8.17	E1	3.07	0.41
E2	274.12	18.59	E2	181.39	5.83	E2	2.04	0.41
E3	267.40	13.86	E3	187.55	11.04	E3	1.61	0.20
E4	288.61	7.77	E4	207.61	12.20	E4	1.64	0.17
E5	276.00	15.61	E5	203.50	7.91	E5	1.42	0.26
E6	275.96	4.59	E6	218.50	4.50	E6	1.11	0.05
I7	264.88	7.36	I7	186.49	6.25	I7	1.43	0.22
I8	289.29	4.15	I8	219.24	6.90	I8	1.24	0.15

The effects of Mg addition on the UTS, YS, and EF of both the T6 and T7 heat-treated non-modified experimental 319 alloys were investigated as a function of aging time, and shown in Figures 11 to 13. Figure 11shows the UTS for non-modified experimental alloys, including the highest recorded UTS value of all the alloys tested here, namely, 462.85 MPa for the non-modified T6-tempered experimental alloy E6 containing 0.6wt% Mg. It was found that alloy strength could be increased by increasing the Mg content. On the other hand, the higher Mg content will also bring about the precipitation of a large volume fraction of the π-$Al_8Mg_3FeSi_6$ phase which ultimately has a deleterious effect on both the strength and the ductility of the alloys. It was also observed that an increase in the Mg content, up to 0.4wt%, at different aging times produces a positive effect on tensile properties, indicating that hardening is due to Mg_2Si precipitation, in addition to the precipitation of Al_2Cu. An increase in the Mg content from 0.3 wt% up to 0.6wt% has hardly any observable effect on the variation in alloy toughness comparative to that reported for other mechanical tests. The effects of Mg in aged alloys are similar to those observed in the as-cast alloys. Aging of these Mg-containing 319 alloys at 180C (356F) in T6 heat treatment conditions for up to 48 hours produces a sharp rise in alloy strength during the first two hours of aging, followed by a broad peak or plateau spread between 2 and 12 hours, as well as a noticeable period of over-aging beyond 12 hours. Aging of these Mg-containing experimental 319 alloys at 220C (428F) in T7 heat treatment conditions for up to 48 hours produces a sharp rise in alloy strength during the first two hours of aging, followed by an aging peak and a noticeable period of over-aging, beyond 2 hours of aging. Figure 13 shows EF (%) for non-modified experimental alloys, in both the T6 and T7 heat-treated conditions, confirming the strength curves plotted in Figures 11 and 12.

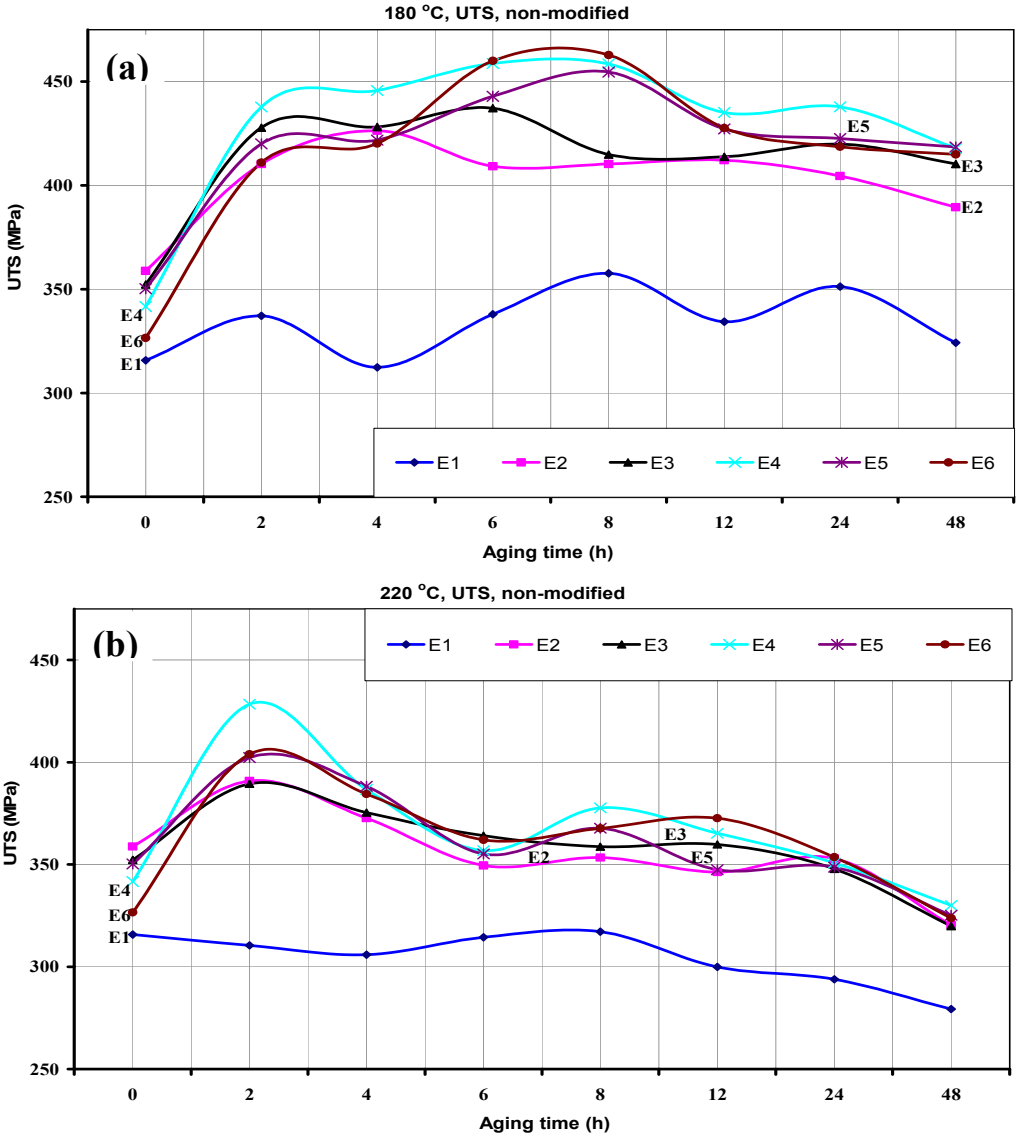

Fig. 11. UTS of experimental non-modified 319 alloys as a function of aging time for: (a) samples T6-tempered at an aging temperature of 180C (356F) and (b) samples T7-tempered at an aging temperature of 220C (428F).

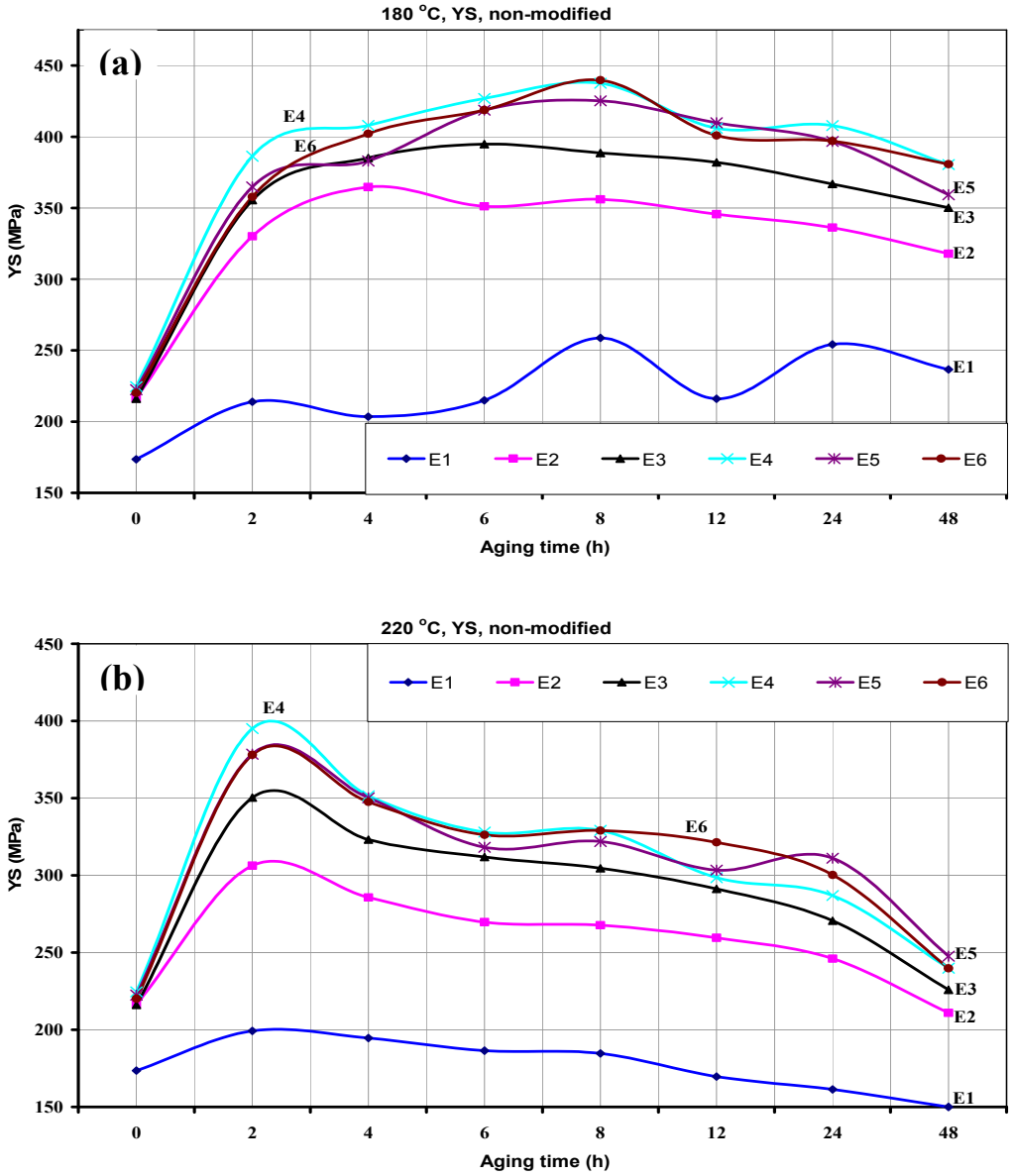

Fig. 12. YS of experimental non-modified 319 alloys as a function of aging time for: (a) samples T6-tempered at an aging temperature of 180C (356F) and (b) samples T7-tempered at an aging temperature of 220C (428F).

The effects of the addition of Mg on the UTS, YS, and EF of the non-modified industrial 319 alloys as a function of aging time were investigated under both T6 and T7 heat treatment conditions. The results are provided in Figures 14 to 16. It was observed that both the Mg-containing industrial and experimental 319 alloys displayed similar behavior with respect to the influence of Mg-content and aging temperature (180C *vs* 220C) (356F *vs* 428F), as shown in Figures 11 through 13. The industrial 319 alloys, however, clearly display lower strength and ductility than the experimental alloys as a result of the presence of tramp elements.

The tensile testing curves shown in Figures 11 to 16 display more than one peak or a wavy form with aging time, resulting from the presence of several hardening phases as reported and explained earlier in the hardness section for the hardness curves.[26]

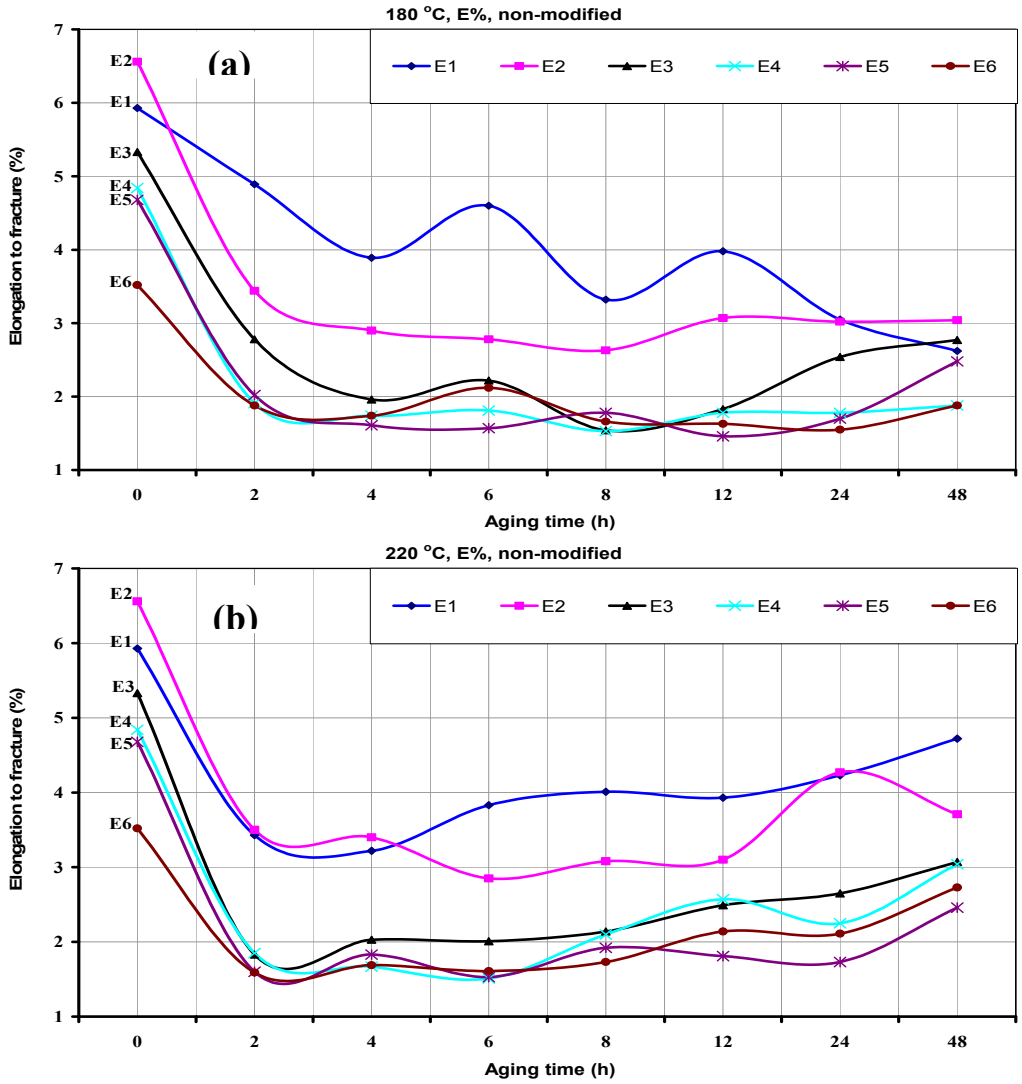

Fig. 13. Elongation to fracture of experimental non-modified 319 alloys as a function of aging time for: (a) samples aged at 180C (356F) and (b) samples aged at 220C (428F).

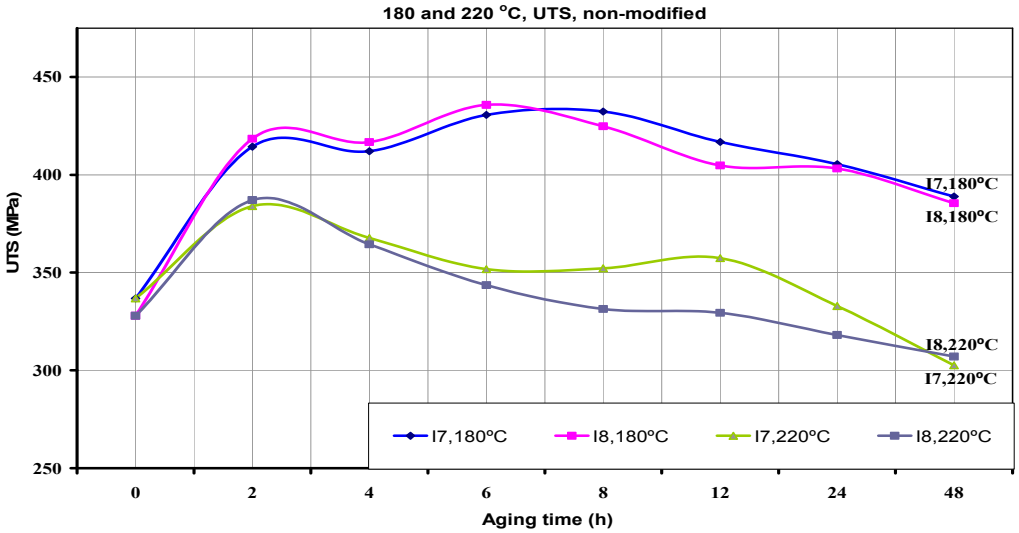

Fig. 14. UTS of industrial non-modified 319 alloys as a function of aging time for both T6-tempered and T7-tempered samples at aging temperatures of 180C (356F) and 220C (428F), respectively.

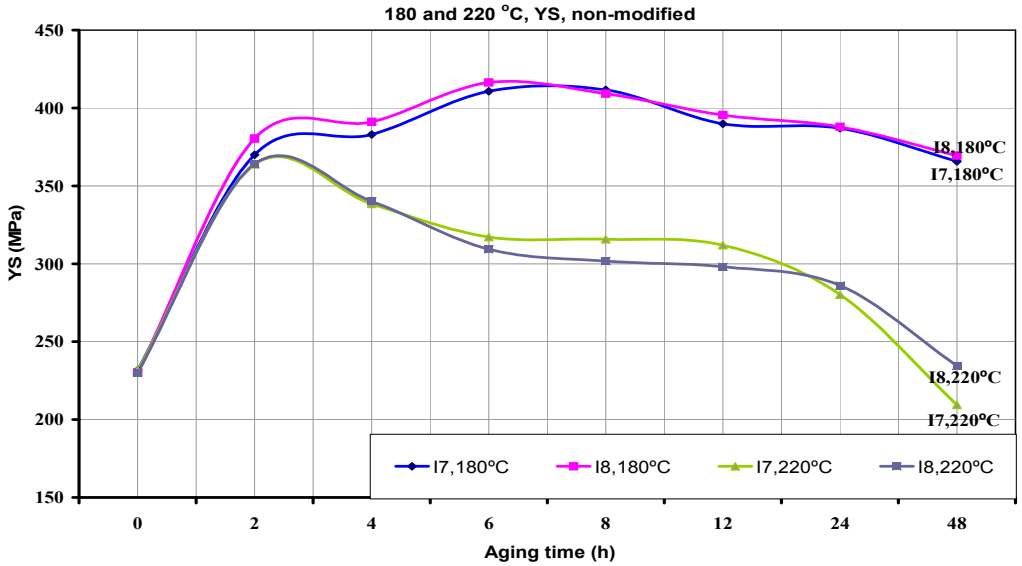

Fig. 15. YS of industrial non-modified 319 alloys as a function of aging time for both T6-tempered and T7-tempered samples at aging temperatures of 180C (356F) and 220C (428F), respectively.

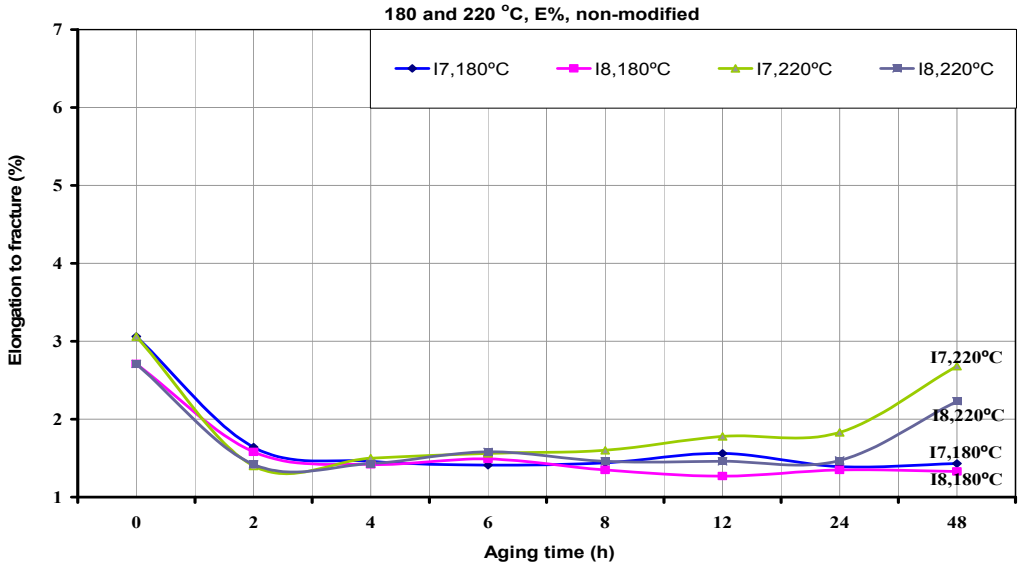

Fig. 16. Elongation to fracture of industrial non-modified 319 alloys as a function of aging time for both T6-tempered and T7-tempered samples at aging temperatures of 180C (356F) and 220C (428F), respectively.

IMPACT TESTING

Tables 9 and 10 summarize the total impact and crack initiation energies of the as-cast alloys tested, respectively. Compared to tensile properties, the cooling rate has a more significant influence on impact properties, *i.e.* impact energy is more sensitive to microstructural changes than are the tensile properties.[29,30] According to these energy values, the impact toughness increases with an increase in cooling rate and decreases with an increase in the Mg content for both the experimental and industrial alloys. The greater part of the total absorbed energy is used for crack initiation, *i.e.* the crack initiation energy is greater than the crack propagation energy, indicating the high ductility of the 319 alloys.

Table 9. Total Absorbed Energy of the As-Cast Experimental and Industrial 319 Alloys

Alloy	E_t (J)		Alloy	E_t (J)	
	Av.	SD		Av.	SD
D1	11.95	3.10	LD1	10.53	1.87
D2	11.74	1.36	LD2	9.41	2.08
D3	8.97	1.49	LD3	7.63	2.03
D4	8.39	1.17	LD4	5.74	0.39
D5	7.94	1.48	LD5	4.91	1.88
D6	6.09	0.79	LD6	3.49	0.82
D7	7.11	0.69	LD7	3.82	1.68
D8	5.42	0.91	LD8	3.42	1.10

Table 10. Crack initiation Energy of the As-Cast Experimental and Industrial 319 Alloys

Alloy	E_i (J)		Alloy	E_i (J)	
	Av.	SD		Av.	SD
D1	8.28	2.87	LD1	7.08	1.69
D2	7.71	1.07	LD2	5.66	1.14
D3	6.29	1.57	LD3	4.47	1.80
D4	4.86	0.75	LD4	3.19	0.27
D5	4.58	1.04	LD5	3.15	1.22
D6	3.33	0.51	LD6	2.13	0.41
D7	4.09	0.43	LD7	2.29	1.01
D8	2.92	0.6	LD8	1.83	0.59

Figures 17 and 18 illustrate the effects of Mg addition on the impact energy values of non-modified experimental 319 alloys as a function of aging time in the T6 heat-treated condition, for samples obtained from the star-like and L-shaped molds, respectively. Figure 17 shows the total impact toughness values for non-modified experimental alloys, including the highest recorded energy value of all the alloys tested, namely 37.5 J, for the non-modified experimental Mg-free alloy D1. It was found that alloy toughness, or the total impact energy, decreased by approximately 39, 41, 42, 43, and 43%, respectively, upon increasing the Mg content (wt%) in the D1 Mg-free base alloy to 0.1 (*i.e.* D2 alloy), 0.2 (D3), to 0.3 (D4), to 0.4 (D5), and finally to 0.6wt% (D6).

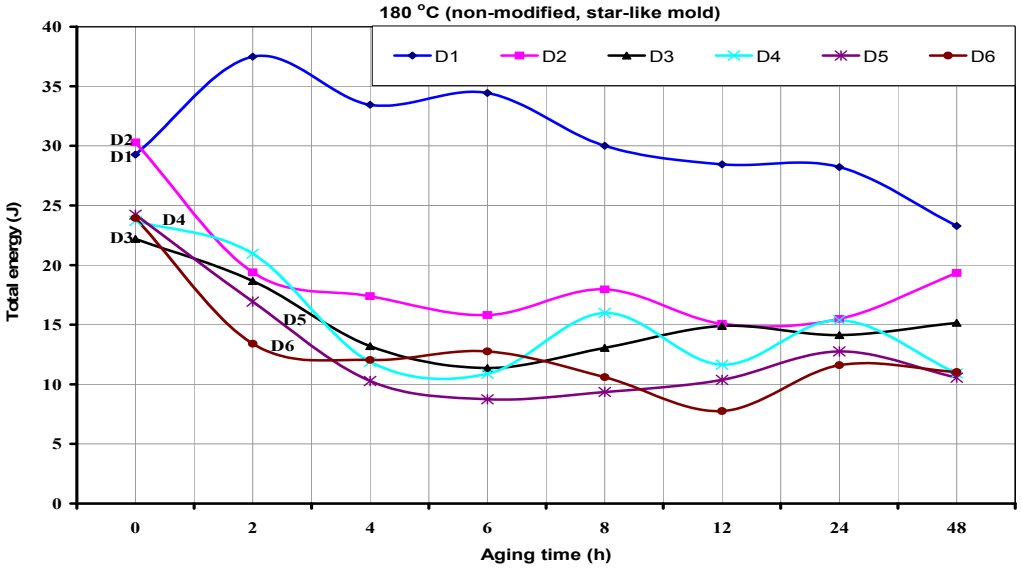

Fig. 17. Total absorbed energy of experimental alloys in the T6-tempered condition at an aging temperature of 180C (356F) for non-modified samples obtained from the star-like mold.

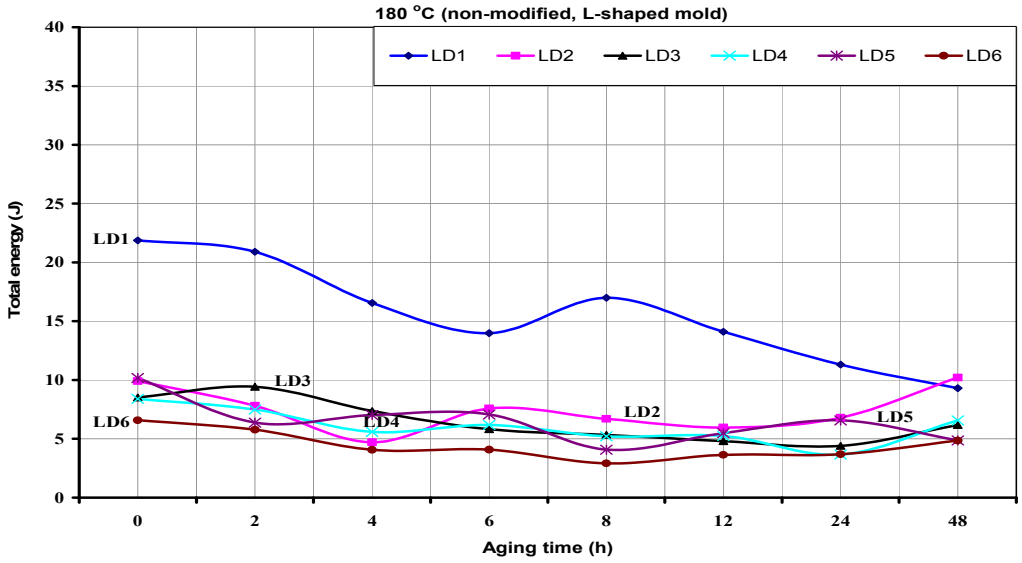

Fig. 18. Total absorbed energy of experimental alloys in the T6-tempered condition at an aging temperature of 180C (356F) for non-modified samples obtained from the L-shaped mold.

An increase of up to 0.4wt% Mg for different aging times was observed to have a negative effect on toughness, demonstrating that Mg has a modifying effect on the Si particles. Magnesium additions also lead to the precipitation of Al_2Cu, which segregates towards areas away from the Si particles. A number of other intermetallics, *e.g.* Mg_2Si, Q-$Al_5Mg_8Cu_2Si_6$, and π-$Al_8Mg_3FeSi_6$, are also formed as the Mg level is increased. Both the insoluble Q-phase and the partially soluble π-phase have a negative effect on impact toughness and fracture behavior. Aging of the 319 alloys at 180C (356F) under T6 heat treatment conditions for up to 48 hours produced a sharp decrease in impact toughness during the first two hours of aging, followed by a broad valley or plateau spread between 2 and 24 hours as well as a noticeable period of overaging beyond 24 hours.

A lower cooling rate L-shaped mold was also used to investigate the effects of the cooling rate parameter on the impact toughness of the experimental 319 alloy containing different amounts of Mg, as shown in Figure 18. Upon comparison with Figure 17, it will be observed that the slow cooling rate diminishes the impact toughness in the T6 alloys; it should be noted that similar observations were recorded by a number of other researchers.[3,29-36] Again, similar observations regarding the negative effects of Mg were made for the low cooling rate samples upon increasing the Mg content.

A report was also compiled concerning the effects that Mg addition would have on the impact toughness of non-modified experimental 319-T7 alloys as a function of aging time. These effects are shown in Figures 19 and 20 for samples derived from the star-like and L-shaped mold, respectively. The effects of the addition of Mg on 319 alloys are closely similar to the ones observed in both the as-cast and T6-treated alloys. The insoluble Q-phase and the partially soluble π-phase, clearly have a negative effect on impact toughness. Under T7 heat treatment conditions, increasing the Mg content also increases the impact energy levels to a greater extent with each increase of additional Mg, compared to the ones observed in the T6 heat-treated conditions. The aging of these Mg-containing experimental 319 alloys at 220C (428F) for up to 48 hours, produced a sharp decrease in hardness during the first two hours of aging, followed by a broad plateau spread between 2 and 24 hours, as well as a noticeable period of overaging beyond 24 hours. Experimental 319-T7 alloys display higher impact toughness than T6-treated alloys as a result of the T7 overaging effect. These observations are all in satisfactory agreement with the work of Ma[31] and Tavitas-Medrano.[37] A greater part of this energy is used for crack initiation, *i.e.* the crack initiation energy is greater than the crack propagation energy, thereby reflecting the high ductility of the 319 alloys investigated.

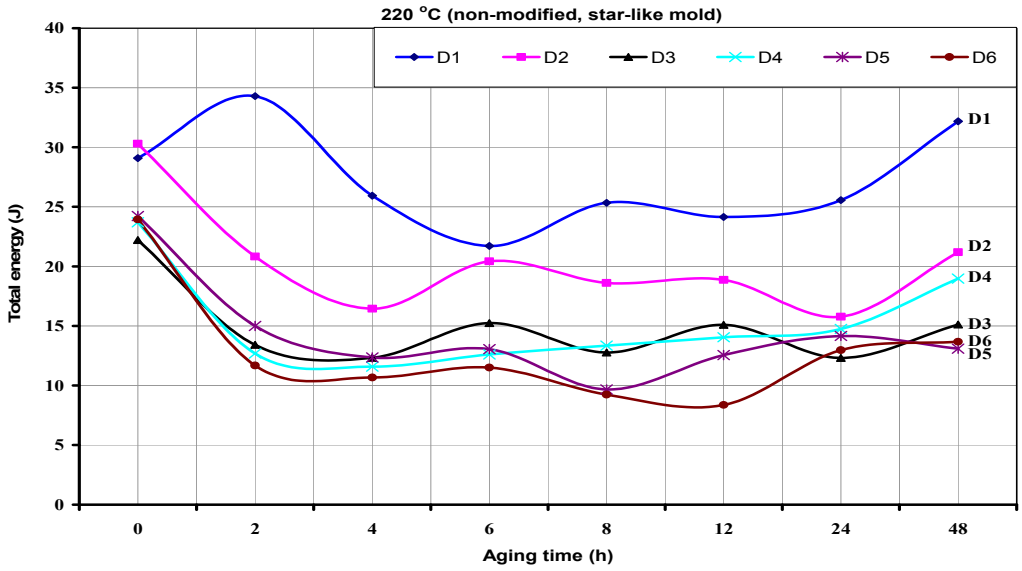

Fig. 19. Total absorbed energy of experimental alloys in the T7-tempered condition at an aging temperature of 220C (428F) for non-modified samples obtained from the star-like mold.

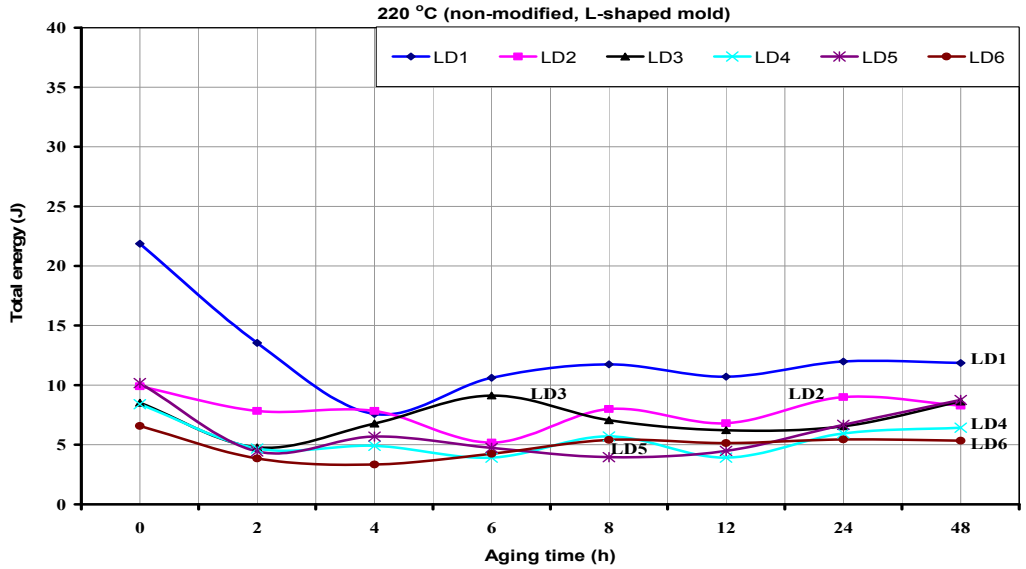

Fig. 20. Total absorbed energy of experimental alloys in the T7-tempered condition at an aging temperature of 220C (428F) for non-modified samples obtained from the L-shaped mold.

Likewise, the effects of Mg addition on the impact toughness of non-modified industrial 319-T6 alloys, as a function of aging time, are shown in Figure 21 for alloy samples obtained from the star-like and L-shaped molds, respectively. The same type of effects were observed for the 319-T7 alloys and are shown in Figure 22 for samples obtained from the star-like and L-shaped molds, respectively. The industrial 319 alloys, however, clearly display lower impact toughness and crack initiation energies than the experimental alloys as a result of the presence of tramp elements. In comparison to the T6 samples, industrial 319-T7 alloys display higher impact toughness values than the 319-T6 industrial alloys as a result of the T7 overaging effects. These observations regarding the industrial alloys confirm the observations noted for the experimental alloys having the same Mg contents and aging conditions. It was also observed that an increase in the Mg content from 0.3 wt% up to 0.6wt% does not have any significant effect on the variation in the alloy toughness similar to the ones reported for other mechanical tests. The impact toughness curves shown in Figures 17 to 22 display more than one peak or a wavy form with aging time, resulting from the presence of several hardening phases as reported and explained earlier in the hardness section for the hardness curves.[26]

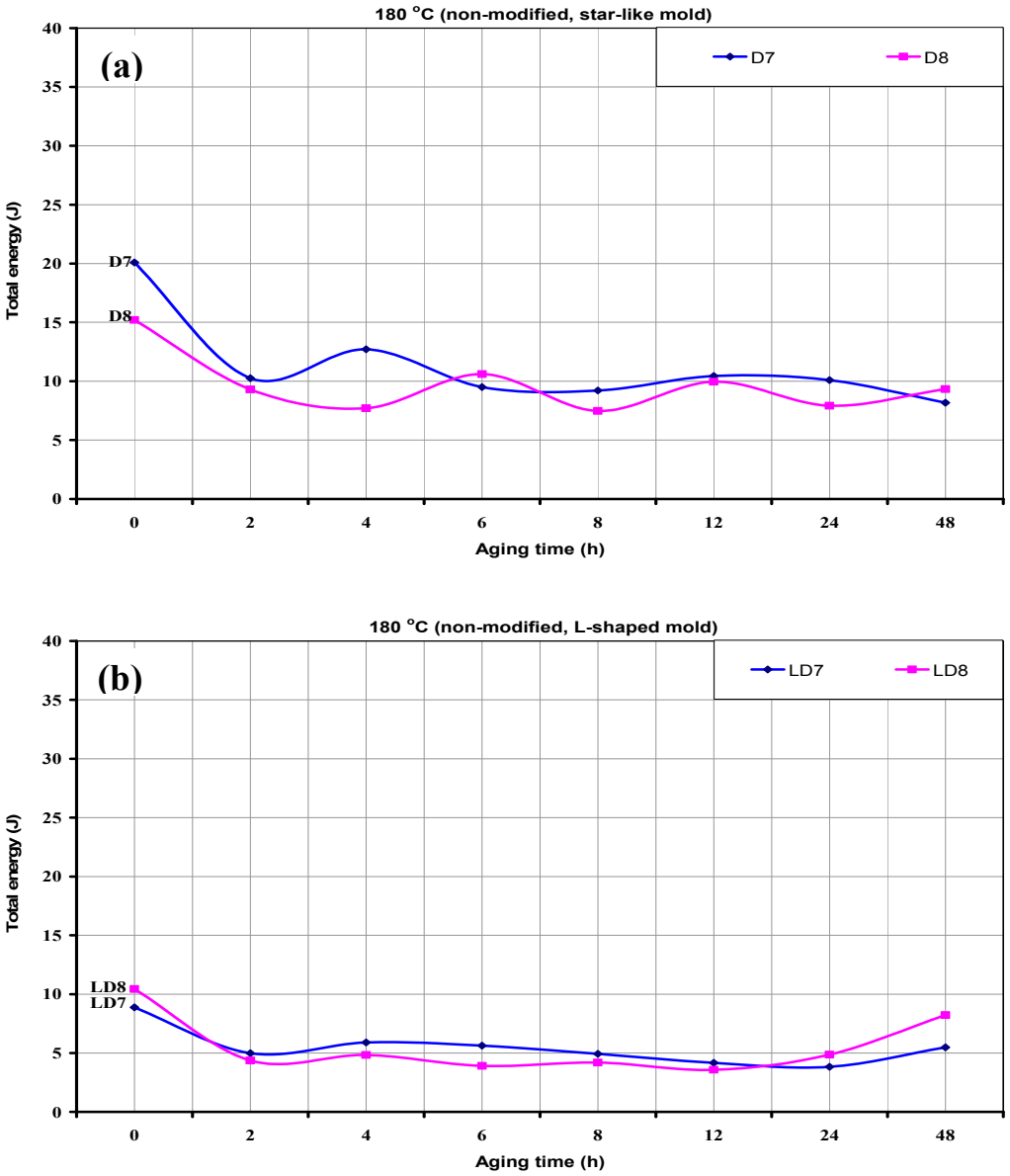

Fig. 21. Total absorbed energy of industrial alloys in the T6-tempered condition at an aging temperature of 180C (356F) for non-modified samples obtained from: (a) a star-like mold, and (b) an L-shaped mold.

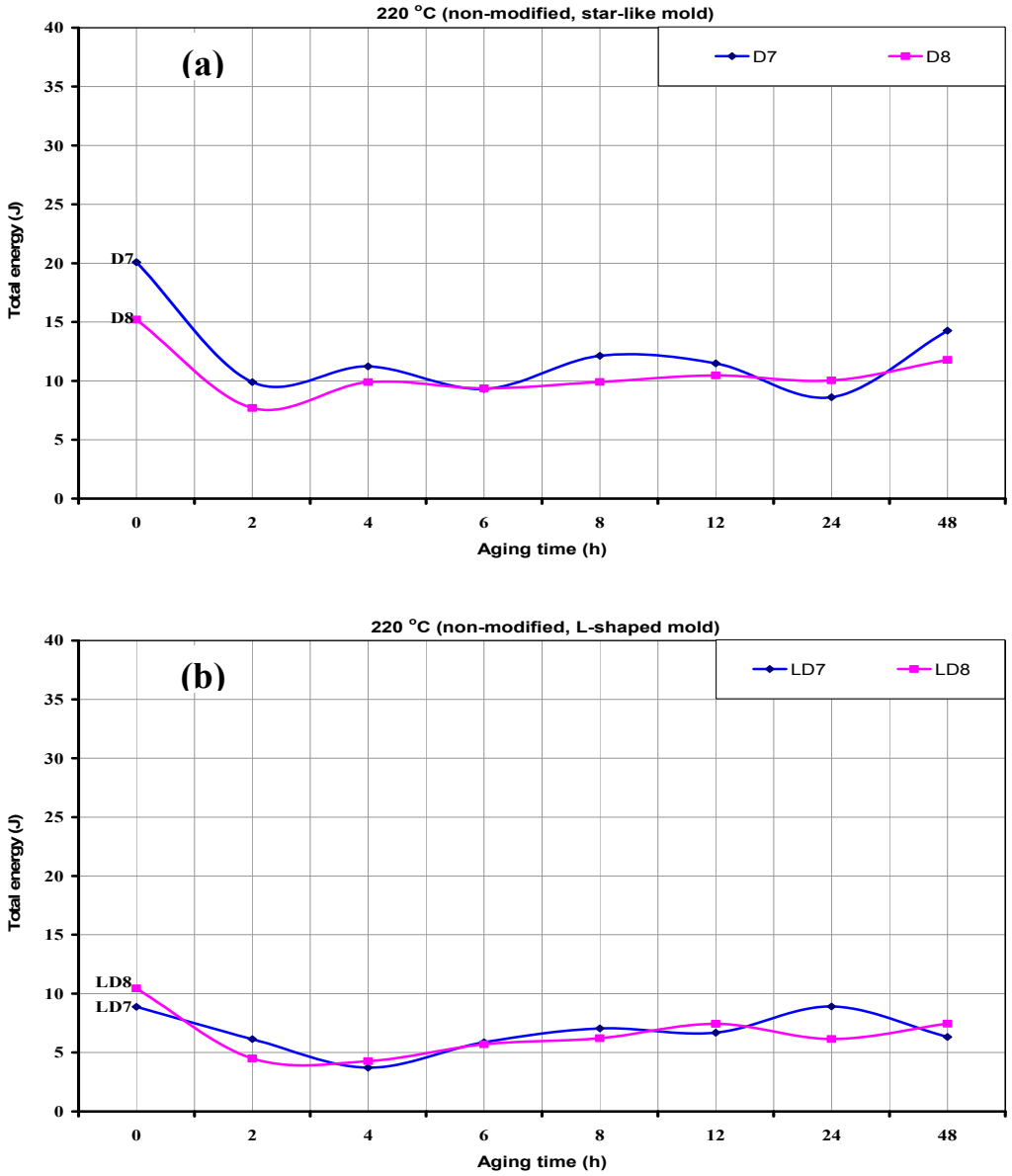

Fig. 22. Total absorbed energy of industrial alloys in the T7-tempered condition at an aging temperature of 220C (428F) for non-modified samples obtained from: (a) star-like mold, and (b) L-shaped mold.

ACKNOWLEDGEMENTS

The authors would like to express their grateful acknowledgement for financial and in-kind support received from the National Sciences and Engineering Research Council of Canada; and from GM Powertrain Group.

CONCLUSIONS

1. The addition of Mg to Fe-containing 319 alloys results in the precipitation of the Mg_2Si, *Q*-$Al_5Mg_8Cu_2Si_6$, and π-$Al_8Mg_3FeSi_6$ phases, where the *Q*- and π-phases appear in a script-like form rather than in irregularly shaped particles.
2. Magnesium and copper improve the hardness and tensile strength of the alloy samples tested, especially in the T6 heat-treated condition. The higher cooling rate also produces an increase in the hardness and tensile strength values.
3. The T7 heat-treated alloys display lower hardness and tensile values than those which were T6 heat-treated. In both T6 and T7 heat-treated conditions, the experimental alloys demonstrate higher hardness values than the industrial alloys.
4. The aging of the Mg-containing 319 alloys at 180C (356F) in T6 heat treatment conditions, as well as of the Mg-containing experimental 319 alloys at 220C (428F) in T7 heat treatment conditions, produces a sharp increase in hardness and tensile strength during the first two hours of aging. At 180C (356F), this initial increase is then followed by a plateau from 2-

12 hours, with a noticeable period of over-aging beyond 12 hours. At 220C (428F), this initial rise is followed by an aging peak and a noticeable period of over-aging beyond 2 hours.

5. The T7 heat-treated alloys displays higher impact toughness values than those that were T6 heat-treated. The experimental 319 alloys demonstrate higher impact energy values than the industrial alloys.
6. Magnesium and copper were observed to decrease the impact toughness of the alloy samples tested, especially under T6 heat treatment conditions due to the segregation of the block-like Al_2Cu phase. The high cooling rate, however, leads to an increase in the impact properties.
7. Aging of the 319 alloys at either 180C (356F) or 220C (428F) produced a sharp drop in impact toughness during the first two hours of aging. For both 180C (356F), and 220C (428F), this initial drop was subsequently followed by a plateau occurring between 2 and 24 hours, with a noticeable period of overaging beyond 24 hours.

REFERENCES

1. Liao, H., Sun, G., *Scripta Materialia*, 48, pp. 1035-1139 (2003).
2. Han, Y.M., Samuel, A.M., Samuel, F.H., Valtierra, S., Doty, H.W., *AFS Transactions*, 116, pp. 79-90 (2008).
3. Paray, F., Kulunk, B., Gruzleski, J.E., *International Journal of Cast Metals Research*, 13, Issue 1, pp. 17-37 (2000).
4. Gruzleski, J.E., Closset, B.M., "The Treatment of Liquid Aluminum-Silicon Alloys," American Foundrymen's Society, Inc., Des Plaines, IL (1990).
5. Tash, M., Samuel, F.H., Mucciardi, F., Doty, H.W., *Materials Science and Engineering A*, 443, pp. 185-201 (2007).
6. Moustafa, M.A., Samuel, F.H., Doty, H.W., *Journal of Materials Science*, 38, pp. 4523-4534 (2003).
7. Mohamed, A.M.A., "Effect of Additives on the Microstructure and Mechanical Properties of Al-Si Alloys," Ph.D. Thesis, Université du Québec à Chicoutimi, Chicoutimi, Canada (2008).
8. Barresi, J., Kerr, M.J., Wang, H., Couper, M.J., *AFS Transactions*, 117, pp. 563–570 (2000).
9. Caceres, C.H., Davidson, C.J., Griffiths, J.R., Wang, Q.G., *Metallurgical and Materials Transactions A*, 30A, pp. 2611-2618 (1999).
10. Wang, Q.G., *Metallurgical and Materials Transactions A*, 34A, pp. 2887-2899 (2003).
11. Durdjevic, M.B., Duric, B., Mitrasinoniv, A., Sokolowski, J.H., *Association of Metallurgical Engineers Serbia and Montenegro*, 9, No. 2, pp. 91-106 (2003).
12. Taylor, J.A., StJohn, D.H., Zheng, L.H., Edwards, G.A., Barresi, J., Couper, M.J., *Aluminium Transactions*, 45, pp. 95-110 (2001).
13. Mbuya, T.O., Odera, B.O., Ng'ang'a, S.P., *International Journal of Cast Metals Research*, 16, No. 5, pp. 451-465 (2003).
14. Taylor, J.A., "The Effect of Iron in Al-Si Casting Alloys", 35th Australian Foundry Institute National Conference, Adelaide, South Australia, pp. 148-157, 31 Oct - 3 Nov (2004).
15. Samuel, A.M., Samuel, F.H., *AFS Transactions*, 100, pp. 657-666 (1992).
16. Bonfield, W., Dutta, B.K., *Journal of Materials Science*, 11, pp. 1661-1666 (1976).
17. Yang, D., "Role of Magnesium Addition on the Occurrence of Incipient Melting in Experimental and Commercial Al-Si-Cu Alloys and its Influence on the Alloy Microstructure and Tensile Properties," Master's Thesis, Université du Québec à Chicoutimi, Chicoutimi, Canada, pp. 57-116 (2006).
18. Gauthier, J., Louchez, P.R., Samuel, F.H., *Cast Metals*, 8, pp. 91-114 (1994).
19. Gauthier, J., Louchez, P.R., Samuel, F.H., *Cast Metals*, 8, pp. 107-114 (1995).
20. Shivkumar, S., Keller, C., Apelian, D., *AFS Transactions*, 98, pp. 905-911 (1990).
21. Samuel, F.H., *Journal of Materials Science*, 33, pp. 2283-2297 (1998).
22. Closset, B., Gruzleski, J.E., *AFS Transactions*, 89, pp. 801-808 (1981).
23. Hatch, J.E., (Ed.), "Aluminum: Properties and Physical Metallurgy," American Society for Metals, Metals Park, OH, (1984).
24. Apelian, D., "Aluminum Cast Alloys: Enabling Tools for Improved Performance," Worldwide Report, NADCA, Wheeling, Illinois, p. 59 (2009).
25. Moustafa, M.A., Lepage, C., Samuel, F.H., Doty, H.W., *International Journal of Cast Metals Research*, 15, pp. 609-626 (2003).
26. Morin, S., "Effet du magnésium, des traitements thermiques et de la porosité sur les propriétés mécaniques de traction et de fatigue de l'alliage sous pression A380.1," M.Sc. Thesis, Université du Québec à Chicoutimi, Chicoutimi, Canada, pp. 137-144 (2002).
27. Paray, F., Gruzleski, J.E., *AFS Transactions*, 102, pp. 833-842 (1994).
28. Tash, M., Samuel, F.H., Mucciardi, F., Doty, H.W., Valtierra, S., *AFS Transactions*, 114, pp. 6-14 (2006).
29. Richard, M., *Fonderie*, 404, pp. 397-400 (1980).
30. Tsukuda, M., Suzuki, T., Fukui, I., Harada, M., *Journal of Japan Institute of Light Metals*, 30, No. 2, pp. 65-71 (1980).
31. Ma, Z., "Effect Fe-Intermetallics and Porosity on Tensile and Impact Properties of Al-Si-Cu and Al-Si-Mg Cast Alloys," Ph.D. Thesis, Université du Québec à Chicoutimi, Chicoutimi, Canada, pp. 158-211 (2002).
32. Hotta, S., Saruki, K., Nakamura, M., *Journal of Japan Institute of Light Metals* (in Japanese), 37, No. 7, pp. 478-482, July (1987).
33. Hafiz, M., Kobayashi, T., *Journal of Japan Institute*

of Light Metals, 44, No. 1, pp. 28-34, Jan. (1994) .
34. Shivkumar, S., Wang, L., Keller, C., *Zeitschrift für Metallkunde*, 85, No. 6, pp. 394-399 (1994).
35. Shivkumar, S., Wang, L., Keller, C., *Journal of Materials Engineering and Performance*, 3, pp. 83-90 (1994).
36. Hafiz, M.F., Kobayashi, T., Fat-Halla, N., *Cast Metals*, 7, No. 2, pp. 103-111 (1994).
37. Tavitas-Medrano, F.J., "Artificial Aging Treatment of 319-Type Aluminum Alloys," Ph.D. Thesis, McGill University, Montreal, Canada, pp. 76-196 (2007).